

Title	Li- and Mg-doping into Icosahedral Boron Crystals, - and - Rhombohedral Boron, Targeting High-Temperature Superconductivity: Structure and Electronic States
Author(s)	Soga, Kohei; Oguri, Atsushi; Araake, Satoshi; Kimura, Kaoru; Terauchi, Masami; Fujiwara, Akihiko
Citation	Journal of Solid State Chemistry, 177(2): 498-506
Issue Date	2004-02
Type	Journal Article
Text version	author
URL	<a href="http://hdl.handle.net/10119/4940">http://hdl.handle.net/10119/4940</a>
Rights	<p>NOTICE: This is the author 's version of a work accepted for publication by Elsevier. Changes resulting from the publishing process, including peer review, editing, corrections, structural formatting and other quality control mechanisms, may not be reflected in this document. Changes may have been made to this work since it was submitted for publication. A definitive version was subsequently published in Kohei Soga, Atsushi Oguri, Satoshi Araake, Masami Terauchi, Akihiko Fujiwara and Kaoru Kimura, Journal of Solid State Chemistry, 177(2), 2004, 498-506, <a href="http://dx.doi.org/10.1016/j.jssc.2003.03.002">http://dx.doi.org/10.1016/j.jssc.2003.03.002</a></p>
Description	

# **Li- and Mg-doping into Icosahedral Boron Crystals, $\alpha$ - and $\beta$ - Rhombohedral Boron, Targeting High Temperature Superconductivity: Structure and Electronic States**

**Kohei SOGA\***, **Atsushi OGURI\*\***, **Satoshi ARAAKE** and **Kaoru KIMURA**

Department of Advanced Materials Science, Graduate School of Frontier Sciences, The University of Tokyo

5-1-5 Kashiwanoha, Kashiwa, Chiba 277-8561, Japan

**Masami TERAUCHI**

Institute of Multidisciplinary Research for Advanced Materials, Tohoku University, 2-1-1 Katahira, Aoba-ku,  
Sendai 980-8577, Japan

**Akihiko FUJIWARA**

School of Materials Science, Japan Advanced Institute of Science and Technology, 1-1 Asahidai,  
Tatsunokuchi, Ishikawa 923-1292, Japan

\*corresponding author

Kohei SOGA (Ph. D.)  
Kiban Bldg. 502/5A5  
5-1-5 Kashiwanoha, Kashiwa  
Chiba 277-8561, Japan  
Tel: +81-4-7136-5457  
Fax: +81-4-7136-3759  
e-mail: mail@ksoga.com

\*\* present address

The Furukawa Electric Co., Ltd., 6 Yawata-kaigandori, Ichihara, Chiba 290-8555, Japan

## Abstract

A possibility of high  $T_c$  superconductivity is suggested for lithium- and magnesium-doped icosahedral boron crystals,  $\alpha$ - and  $\beta$ -rhombohedral boron. The doping of these elements were attempted by a vapor diffusion processing. Both of lithium and magnesium are hardly doped into the  $\alpha$ -rhombohedral boron, though small amount of metallic parts were found in the sample. In only one sample, the metallic part contained 0.02 vol% of superconductive phase ( $T_c \sim 36\text{K}$ ). Magnesium was successfully doped into  $\beta$ -rhombohedral boron homogeneously up to 4 at% ( $\text{Mg}_{4.1}\text{B}_{105}$ ), though considerable amount of impurity silicon was introduced together with magnesium. The structures of the doped samples were analyzed assuming co-doping of magnesium and silicon. The relation between the site occupancies of the dopants and the lattice expansion is discussed. The estimation of the density of states near the Fermi energy by EELS and magnetic susceptibility measurements suggested a metal transition of the  $\beta$ -rhombohedral boron by the doping of magnesium and silicon. The relation between the metal transition and the intrinsic acceptor level is also discussed.

## I. Introduction

Pure boron (B) solids, such as  $\alpha$ - and  $\beta$ -rhombohedral B ( $\alpha$ -B,  $\beta$ -B) or amorphous B (a-B), are cluster solids which consist of icosahedral  $\text{B}_{12}$  clusters. In the framework that consists of the  $\text{B}_{12}$  clusters, they have considerably large interstitial doping sites, where they can contain several and up to twenty at% of other elements as dopants and components for  $\alpha$ -B and  $\beta$ -B, respectively, without destructing the original structure in the un-doped form [1-15]. We have reported that the doping of metallic elements into these sites reveals interesting variety of the change in physical properties of  $\beta$ -B [16-19] and a-B [20, 21]. For example, three major doping sites are known for  $\beta$ -B, which are called  $A_1$ , D and E sites [16, 17]. The occupation of a site depends on the element to be doped. Vanadium (V) only occupies the  $A_1$  site and lithium (Li) does only the D and E sites. Copper (Cu) and nickel (Ni) are intermediate. Another notable character of  $\beta$ -B is the existence of an intrinsic acceptor level (IAL) in the band gap right above the valence band, which is suggested to accept 8 electrons per  $\text{B}_{105}$  rhombohedral unit cell [16]. One of the interesting changes of physical properties mentioned above is of the electrical conductivity. In the case of Li-doping, the maximum number of the doped Li atoms for  $\beta$ -B is 8 per  $\text{B}_{105}$ . The electrical

conductivity once increases by the lithium doping, which is due to the donation of one electron from each Li atom into the IAL. However, after the doping of about the half of the IAL, the conductivity begins to decrease and the sample reaches back to a semiconductor by doping 8 lithium atoms. This decrease is explained as the filling up of the IAL, which dominates the conductivity by the doped electrons. In the case of Li-doping without occupation of  $A_1$  site, a band structure of the band gap with the IAL seems to hold after the doping, i.e. a rigid band scheme is valid. On the other hand, the V-doping into the  $\beta$ -B increase the conductivity much more than Li-doping and a metal transition may occur with only about 1 at% of V-doping. This is the case of  $A_1$  site occupation and the rigid band scheme does not hold for this case. For Cu and Ni doping, the behaviors are intermediate between those of Li and V. Thus, the electrical conductivity of doped  $\beta$ -B is dominated by the kinds of doping sites and dopant elements.

Another remarkable character of icosahedral cluster solids is possibility of relatively higher density of states (DOS) near the Fermi energy due to the high symmetry of the cluster unit. The high symmetry of the  $B_{12}$  cluster, icosahedral symmetry, give rise high degeneracy of the electronic states, which accordingly results in the high DOS. If one can adjust the Fermi energy to the energy with the above high DOS, there is a possibility of higher critical temperature ( $T_C$ ) of superconductivity for the icosahedral cluster solid. Gunji et al. [22, 23] performed a first-principle study on  $Li_xB_{12}$  solids and predicted the superconductivity of Li-doped  $\alpha$ -B. Table 1 shows the comparison of the solids with layered structures and the cluster solids. In the case of carbon (C) rich solids, a graphite intercalation compound  $KC_8$  has a layered structure with the DOS at the Fermi energy ( $N(E_F)$ ) of 14.3 (states/eVnm<sup>3</sup>) [24] and  $T_C$  is 0.1 K. On the other hand,  $K_3C_{60}$  is a cluster solid consists of  $C_{60}$  clusters, which have the same icosahedral symmetry as  $B_{12}$  clusters. A doped fullerene solid  $K_3C_{60}$  has much higher  $N(E_F)$  of 25.3 (states/eVnm<sup>3</sup>) [25, 26] and  $T_C$  of 20 K than those for layered  $KC_8$ . In the same reason, B-rich icosahedral cluster solids should have higher  $T_C$  than the layered structure B-rich solids. Typical B-rich solids with layered structure are diborides, which have the same honeycomb layers as graphite.  $MgB_2$  is one of diborides and has the  $T_C$  of 39 K [27]. The reasons for the much higher  $T_C$  of  $MgB_2$  than that of  $KC_8$  with the similar structure are as follows. One of them is the higher  $N(E_F)$  of 24.4 (states/eVnm<sup>3</sup>) for the  $MgB_2$  [28]. We can expect higher value for the B-rich cluster solids as seen from the result calculated by Gunji et al. for  $Li_xB_{12}$  ( $N(E_F)=39.3$  (states/eVnm<sup>3</sup>)) [23].

Other reasons of high  $T_C$  for  $\text{MgB}_2$  are related to the electron-phonon interaction [28, 29]. The B-rich solids have phonon modes with a high frequency, since boron is a light element similar to carbon, which is as desirable as the case of C-rich solids. The Fermi energy of  $\text{KC}_8$  is located in a  $\pi$ -band, while that of the  $\text{MgB}_2$  is located in mixture of  $\sigma$ - and  $\pi$ -band. The  $\sigma$ -band electrons at the Fermi energy can be coupled with B-B stretching mode which have higher frequency and stronger coupling constant than C-layer bending mode which is coupled with the  $\pi$ -band electrons. The same situation may apply for the case of cluster solids. Furthermore, the B-rich cluster solids are thought to have strong electron-lattice interaction, which is supported by the observed bipolaron hopping conduction for one of them,  $\text{B}_4\text{C}$  [30].

The above comparison leads us to expect much higher  $T_C$  for the B-rich cluster solids than the layered  $\text{MgB}_2$ . According to the BCS theory, the  $T_C$  is roughly expressed as

$$T_c \propto \omega \exp\left(-\frac{1}{VN(E_F)}\right), \quad (1)$$

where  $\omega$  is the phonon frequency and  $V$  is the electron-phonon coupling constant. As described above, all of the three factors,  $\omega$ ,  $V$  and  $N(E_F)$ , of B-rich icosahedral cluster solids act desirable to accomplish a high  $T_C$ .

We reported a study on the Li-doping on the  $\beta$ -B [16]. As shortly described above, the Li-doping only filled up the IAL and we could even not observe a metal transition. Magnesium (Mg) is an element, which has the similar atomic radius as the Li and may donate double number of electrons to the  $\beta$ -B since a stable Mg ion is a divalent ion. Thus, we can expect to push the Fermi energy above the IAL into the conduction band with much less number of Mg than the case of Li. In the present study, we report the study on the Li-doping to  $\alpha$ -B and Mg-doping to  $\alpha$ - and  $\beta$ -B. The structure and electronic states, together with magnetic and superconductive properties of the doped B will be discussed.

## II. Experimental

The  $\alpha$ -B was prepared by crystallizing amorphous B (a-B) powder with 3N purity, which is similar method reported in the literature [31, 32]. The a-B powder placed in a tantalum tube with 3N purity was sealed in

a quartz tube with argon gas with 18.7 kPa pressure. The tube was heated up to the temperature of 1200 °C and maintained for 10 hrs. The formation of the  $\alpha$ -B was confirmed by an x-ray diffraction (XRD). As for the  $\beta$ -B, commercial 2N and 5N powders were used.

Li or Mg was doped in to  $\alpha$ - or  $\beta$ -B by a vapor diffusion processing (VDP), which is essentially the same way used for the Li-doping into  $\beta$ -B [16].  $\alpha$ - or  $\beta$ -B powder was placed on one side and bits of Li and Mg with 3N purity on the other side of a tantalum or boron nitride reaction tube. The reaction tube was sealed in an evacuated quartz tube doubly and singly for Li and Mg, respectively, and heated up and kept at varied temperatures between 700 °C and 1300 °C for a desired time.

The samples are examined by an XRD with Cu-K $\alpha$  radiation in the  $2\theta$  range from 10 to 80 degree. The lattice constants were determined by analyzing the peaks between 37 and 57 degree, calibrating the angle using silicon powder mixed with the samples in this measurement. The XRD patterns of doped and un-doped  $\beta$ -B were analyzed by the Rietveld method to determine the site occupancies of dopants. A program RIETAN2000 was used for the Rietveld refinement [33].

Electron energy-loss spectroscopy (EELS) was applied for the samples to obtain information of the density of states (DOS) of the conduction band. A specimen-cooling holder with liquid nitrogen was used and the recording time was set as short as 90 seconds -for the Li-doped sample to avoid the evaporation of Li from the doped sample by electron beam irradiation. Mg doped sample was stable under the electron beam irradiation. The details of the EELS measurement were described in other papers [34, 35].

The magnetic susceptibility of the samples was measured by using a superconducting quantum interference device (SQUID) magnetometer. The sample was first cooled to 2 K under a zero field and the signal was recorded under a field during warming (zero-field cooled, ZFC). Then the signal was recorded under the same field during the cooling down to 2 K (field-cooled, FC). The applied strength of the magnetic field was 10 Oe for the examination of superconductivity and 10000-50000 Oe for the observation of other magnetic properties.

### III. Results and Discussion

## A. Li- and Mg-doping on $\alpha$ -rhombohedral boron

Doping of Li and Mg into  $\alpha$ -B was attempted by the VDP. Fig. 1 shows the conditions for the VDP. The temperature was set to be at 900~1220 °C for Li-doping and at 700-1220 °C for Mg-doping. The samples were kept at the temperatures for 2~70 hours. Fig. 2 shows the typical XRD patterns of the samples denoted as Li- $\alpha$ -1 and Mg- $\alpha$ -1 in Fig. 1 together with that of un-doped  $\alpha$ -B. The XRD patterns are almost the same for all samples. None of the peaks of stoichiometric lithium or magnesium borides was found, though the small peaks of impurities as  $\beta$ -B, B<sub>6</sub>O and TaB<sub>2</sub> were detected beside the peaks of  $\alpha$ -B. The origin of TaB<sub>2</sub> is the contamination from reaction of the boron powder with the Ta tube. The changes in peak positions and intensities due to the VDP were under detection for all samples. This fact means that Li and Mg were not doped in whole sample for  $\alpha$ -B not like for  $\beta$ -B described in the next section.

The colors of the samples were mostly red, which is the color of  $\alpha$ -B. Only some parts of samples showed metallic glittering. We picked out the glittering particles and examined under a TEM equipped with an EELS measurement system. The patterns of Bragg spots from the particles were almost the same as that of un-doped  $\alpha$ -B. Fig. 3 shows the results of the EELS measurement [34] together with the DOS of un-doped  $\alpha$ -B obtained by using first-principle calculation, which was quoted from the paper by Gunji et al. [23]. The spectrum of pure  $\alpha$ -B agreed well with the calculated DOS of the conduction band. By the VDP of Li and Mg, the main peaks at 191 eV shifted to the lower energy. This chemical shift and the appearance of the Fermi edge mean the increase of the electrons in the conduction band. More precise reading of the EELS data is described in ref. [34].

The glittering and the chemical shift of the particles suggest a metal transition of  $\alpha$ -B due to the doping of Li and Mg, though the change of the XRD pattern was under detection since the doping was only partial. To examine the superconductivity, we performed a magnetization measurement for the samples. We could not observe superconductivity except the only one sample, Li- $\alpha$ -1. Fig. 4 shows the temperature dependence of magnetic susceptibility,  $\chi$ , of un-doped  $\alpha$ -B and the sample Li- $\alpha$ -1 under conditions of zero field cooling (ZFC) and field cooling (FC) at a magnetic field of 200 Oe [36]. A drop of the  $\chi$  observed for the Li- $\alpha$  under the ZFC seems to be due to the shielding effect. The positive shift of the  $\chi$  for the Li- $\alpha$  should be originated from an unknown

ferromagnetic impurity. The  $T_C$  is estimated to be 36 K, which is slightly lower than  $T_C = 39$  K for  $MgB_2$  [27]. The estimated volume fraction for the superconductive phase to the whole sample was only 0.02 %. The magnetization under varied magnetic field above and below the  $T_C$  is shown in Fig. 5 [36]. The magnetization at 100 K was subtracted from both of the values at 20 and 37.5 K to eliminate the temperature independent component due to the ferromagnetic impurity. The magnetization at 20 K is negative under a weak magnetic field and approaches to the value at 37.5 K by increasing the magnetic field. This result suggests that the drop of the  $\chi$  in Fig. 3 is caused by the shielding effect. The increase of the magnetization at 37.5 K is due to the temperature dependent Curie-Weiss term and will be discussed in the later section for  $\beta$ -B. We should wait for the development of the synthesis method of Li or Mg-doped  $\alpha$ -B and not assert that the superconductive phase is Li-doped  $\alpha$ -B since the volume fraction of the phase is too small.

#### B. Structure of Mg-doped $\beta$ -rhombohedral boron

Mg was doped successfully into  $\beta$ -B with 2N purity by the VDP. The VDP temperature was fixed to be at 1200 °C. The amount of the doped Mg was a few percent by the VDP for 10 hrs. To dope more Mg, we applied longer VDP time up to 200 hrs or multiple doping of 10hrs up to 7 times. The VDP conditions are listed in Table 2. We use the sample name listed in the table to denote a sample in the following part. As results of the XRD, the lattice constants and volumes of the hexagonal unit cell were also listed in the table. The a-axis and c-axis expanded up to 1.26 and 0.68 % by the doping, respectively. The XRD patterns of un-doped  $\beta$ -B and Mg- $\beta$ -1 as an example of doped samples are shown in Fig. 6. Though the shifts and intensity changes of the peaks were observed, we found that the framework of the  $\beta$ -B was remained after Mg doping since the overall profile did not change essentially. To confirm the doping of Mg, an energy dispersive spectroscopy (EDS) was performed for some of the samples. As a result, considerable amount of silicon (Si) was doped in the sample beside the Mg. The source of the Si may be that from the quartz tube used for the VDP because Mg is a strong reducer and quartz should be reduced to form atomic Si. Therefore, we carried out the Rietveld refinement on the XRD patterns of the Mg- $\beta$ -1~11 assuming co-doping of Mg and Si.



For the Rietveld refinement of the crystal structure, we selected the doping site of Mg and Si atoms according to literature. In the following part, the notation of the site is according to those in literature [1, 37, 38]. The site occupancies of various dopants are listed on Table 3. We assumed the sites for Si to be the  $A_1$ ,  $A_2$  and B(1) since Vlasse et al. reported [1] that Si atoms occupy these sites in the  $\beta$ -B. Then we eliminated the  $A_2$  site from the Si sites after several trials since the assumption of the occupancy of Si at  $A_2$  were negative. Recently, the dope sites of Mg have been reported to be D, E and F [37]. As seen from the Table 3, all of the metal atoms occupy  $A_1$ , D, E or F sites. Also, atoms larger than aluminum do not occupy  $A_1$  site. Therefore, we assumed D, E and F sites as the dope sites for Mg. For the simplicity of the analysis, all of the interstitial sites of B, B(N) with  $N > 15$ , were neglected. The site occupancies of Si and Mg are listed on Table 4 together with the  $R_{wp}$ , which is a measure of the refinement quality [10, 40]. The occupancy of B at B(13) is also listed, which is known to be ~75 % for pure  $\beta$ -B [38]. The values of  $R_{wp}$  (9~11 %) are comparable or less than those reported for  $LiB_{13}$  (11~17 %) [10]. Fig 7 shows the relation between the total doping time and site occupancies. On the first stage, the occupancies of Mg at both D and E sites increase by up to 40 hrs. After 40 hrs, the occupancy of Mg decreases and that of Si increases. The occupancies of Si at the B(1) site and Mg at the E site behaved oppositely. In the same way, the behavior of the occupancies of Mg and B at B13 site were opposite. Fig. 8 shows the schematic illustration of the above sites in  $\beta$ -B. The B(1) sites are in between the  $A_1$  and E sites. On the first stage, Mg occupies the D, E and F sites and then Si atoms take place to be doped at the  $A_1$  or B(1) site. After 40 hrs doping, the Si atoms ejected the Mg atoms because the doping to both of Si in the B(1) and Mg in the E sites may cause too much tension to the structure since the atomic radius of Si is larger than that of B. Finally, by the continuous doping of silicon up to 100 hrs, the E site with Mg was emptied. The reason of the decrease of Mg at the D site is not clear but the anisotropic cell expansion due to Si doping opposite from that due to Mg may cause the tension to eject the Mg from the D site. The relation between the cell expansion and the site occupancies will be discussed later. In the same way, when the occupancy of Mg at the D and F sites increased, the neighbor B atoms at B(13) and B(4) sites may be ejected to relax the structure. For B(13) deficiency naturally occurs even for pure  $\beta$ -B.

In Fig. 9 (a) and (b), the expansion of the cell measured by the peak positions of XRD patterns and the number of doped Mg and/or Si obtained by the Rietveld refinement were correlated. As seen from Fig. 9(a), the

doping of both Mg and Si caused the expansion of the cell to the a-axis orientation. Also, the figure clearly shows that the ejection of Mg was mainly caused by the doping of Si at the B(1) site. On the other hand, the only correlation found for the a-axis expansion was a linear correlation between the number of Mg at D site and Si at B(1) site. To separate the effects of Si- and Mg-doping, we assumed a linear correlation between the dopant contents and the lattice constants, and applied a least square fit to the observed lattice constants using the equations

$$\begin{aligned} a &= f_{\text{Si}}^a x_{\text{Si}} + f_{\text{Mg}}^a x_{\text{Mg}} + a_0 \\ c &= f_{\text{Si}}^c x_{\text{Si}} + f_{\text{Mg}}^c x_{\text{Mg}} + c_0 \end{aligned}, \quad (2)$$

where  $a$ ,  $c$  are the lattice constants,  $a_0$ ,  $c_0$  are lattice constants of un-doped  $\beta$ -B,  $x_M$  is the content of dopant M in at% obtained by Rietveld refinement and  $f_M^{a \text{ or } c}$  are linear coefficients, which were obtained as fitting parameters. The results of the fitting are shown in Fig 9 (c). The correlation coefficients were 0.99 for both a- and c-axis. The correspondence of the site occupancy obtained by Rietveld refinement and the lattice constants obtained from the peak positions of XRD patterns support the reliability of the results of the Rietveld refinement. The obtained linear coefficients as fit parameters are  $f_{\text{Si}}^a = 3.99 \times 10^{-2}$ ,  $f_{\text{Mg}}^a = 1.00 \times 10^{-2}$ ,  $f_{\text{Si}}^c = 2.17 \times 10^{-2}$  and  $f_{\text{Mg}}^c = 6.98 \times 10^{-2}$  ( $\text{\AA}/\text{at}\%$ ). These values are comparable to those obtained for single element doping from the literature,  $f_{\text{Si}}^a = 3.27 \times 10^{-2}$ ,  $f_{\text{Si}}^c = 1.09 \times 10^{-2}$  [1],  $f_{\text{Mg}}^a = 0.91 \times 10^{-2}$  and  $f_{\text{Mg}}^c = 7.39 \times 10^{-2}$  ( $\text{\AA}/\text{at}\%$ ) [37]. The doping of Si has  $\sim 3$  times more effect on the a-axis expansion. On the other hand, Mg-doping affected on the c-axis expansion  $\sim 3$  times more than Si-doping. Thus, we conclude that the doping of Si and Mg are effective to the expansions of the cell in a-axis and c-axis directions, respectively.

### C. Electronic states and magnetic properties of Mg-doped $\beta$ -rhombohedral boron

Fig. 10 shows the results of EELS measurements [35] on  $\beta$ -B, Mg- $\beta$ -1, 3 and 8. A stepwise increase of the signal was observed for the samples Mg- $\beta$ -3 and 8 around 188.5 eV. We can take this as a discontinuous increase of the signal since the resolution of the measurement is 0.26 eV. This discontinuous increase of the signal is due to the formation of Fermi edge in the conduction band. The formation of Fermi edge suggests the possibility of metal transition of  $\beta$ -B by the Mg-doping. More precise reading of the EELS data is described in ref.

[35].

Temperature dependencies of magnetic susceptibility,  $\chi$ , of selected samples were measured to investigate the Mg-doping effects on the electronic states. The results are shown in Fig. 11. Though no transition due to superconductivity was observed, the samples showed temperature dependent magnetism.  $\chi$  of a substance at a temperature  $T$  can be fitted as

$$\chi = \chi_0 + \chi_{CW} = \chi_0 + \frac{C}{T - \theta_p}, \quad (3)$$

where  $\chi_0$  is a temperature independent part. The second term is a temperature dependent part obeying Currie-Weiss (CW) law, where  $\theta_p$  is the Weiss temperature. The  $C$  is the Currie constant and described as

$$C = \frac{N\mu_B^2 p_{\text{eff}}^2}{3k_B}, \quad (4)$$

where  $p_{\text{eff}}$  is the effective Bohr magneton and  $N$  is the spin density. The contribution of  $\chi_{CW}$  increased by increasing the Mg content. The data in Fig. 12 was completely fit by eq. (3) and  $\chi_0$ ,  $C$  and  $\theta_p$  were obtained as fitting parameters for each sample. The results are shown in Table 5. To investigate the origin of this  $\chi_{CW}$ , we also measured the  $\chi$  of pure  $\beta$ -B with 5N purity, for which  $\chi_{CW}$  was not observed. Thus, the Mg-doping may not be only the origin of  $\chi_{CW}$  but the impurity in  $\beta$ -B with 2N purity is also a possible reason of the CW component. A major impurity in 2N  $\beta$ -B is 0.1 wt% of Mg, which corresponds to 0.05 at%. Therefore, it is natural to think that the origin of  $\chi_{CW}$  is the Mg-doping. It is reported that the dopants at A<sub>1</sub> or D site forms a pair and originate an antiferromagnetism for  $\beta$ -B doped with manganese or iron [40, 41]. In the present case of Mg-doping,  $\theta_p$  is also negative but very small, and antiferromagnetic coupling between local moments is negligible. Though Mg atoms or ions are not a magnetic element, the electrons doped into B framework may produce local moments. The spin density,  $N$ , in eq. (4) should be proportional to the dopant concentration. Fig. 12 shows the relation between the dopant content at each site and  $C$ . Obviously, only the content of Mg at D site showed a linear correlation with  $C$ . Thus, the other dopants than Mg at the D site are not the origin of the observed CW component. Another possibility is the impurity contained not only in B but also in Mg used for the VDP, which may be introduced into the samples together with Mg, because the CW component increased after the Mg-doping. According to the report of the supplier, the used Mg metal contains 0.01 Zn, 0.007 Si, 0.007 Al, 0.004 Fe, 0.004 Mn, 0.001 Cu and 0.001

Ni in wt%. Among them, most effective element for ferromagnetism is Fe. We examined the content of the Fe in Mg- $\beta$ -6 and 10 by using an inductively coupled plasma (ICP) measurement. The content was 0.03 wt% for both. Assuming that the  $p_{\text{eff}}$  of Fe<sup>3+</sup> and Fe<sup>2+</sup> are 5.8 and 5.2, respectively, we calculated the corresponding content of Fe to the values of  $C$ . The resulted values are ranged between 0.1 and 0.2 wt%, which are much larger than the content obtained by the ICP. Also, the value of  $C$  for Mg- $\beta$ -6 is almost double of that for Mg- $\beta$ -10 though the content measured by ICP was same for the both. Thus, the amounts of the impurities from the Mg source are too small to explain the appearance of the CW component.

The temperature independent part,  $\chi_0$ , contains diamagnetism because the  $\chi$  is negative even at room temperature.  $\chi_0$  can be written as

$$\chi_0 = \chi_p + \chi_L + \chi_d, \quad (5)$$

where  $\chi_p$  is due to the Pauli paramagnetism,  $\chi_L$  the Landau diamagnetism and  $\chi_d$  the closed-shell diamagnetism including Larmor diamagnetism. Among them, the  $\chi_d$  is not supposed to be affected by doping of metals. Accordingly, one can express  $\Delta\chi_0$ , which is the change of the  $\chi_0$  due to the doping, as

$$\Delta\chi_0 = \Delta\chi_p + \Delta\chi_L = \frac{2}{3} \mu_B^2 \Delta N(E_F), \quad (6)$$

where  $\Delta N(E_F)$  is the difference of the  $N(E_F)$  from that of the un-doped sample. Therefore, the dependence of  $\Delta\chi_0$  on the dopant content corresponds to that of  $\Delta N(E_F)$ . The  $\Delta N(E_F)$  can be approximately taken as  $N(E_F)$  because the un-doped  $\beta$ -B is semiconductor, whose  $N(E_F)$  is nearly zero. As described in the introduction, the number of electrons donated by the dopants has important meaning for the metal transition of doped  $\beta$ -B because we can expect that the donated electrons fill up the IAL and Fermi energy will reach to the conduction band. The capacity of IAL is 8 electrons/B<sub>105</sub>. By assuming that each Mg atom donates 2 electrons and the Si atom doped at B1 by replacing a B atom donates one electron, we can calculate the number of doped electrons from their site occupancies. Fig. 13 shows the relation between the  $\Delta N(E_F)$  and the number of doped electrons. The  $\Delta N(E_F)$  increases at the total number of electrons more than 8. The sample names indicated in the figure with arrows correspond to those used for the EELS measurement. As discussed above, the appearance of Fermi edge indicated the metal transition only for the samples Mg- $\beta$ -3 and 8. The total number of electrons for Mg- $\beta$ -1 (6.2) is less than

8. On the other hand, the numbers for Mg- $\beta$ -3 and 8 are 8.9 and 8.6, respectively. The number of doped electrons for Mg- $\beta$ -8 only from the Mg atoms is 6.6, which is less than 8 though both of the results of the EELS measurement and the  $\Delta N(E_F)$  shows that metal transition occurred for the sample. Thus, we conclude that more than 8 electrons donated both from the Si atoms at the B1 site and Mg atoms pushed the Fermi energy above the IAL and caused the metal transition.

#### IV. Conclusion

Doping of Li and Mg into  $\alpha$ -B was attempted by the VDP. The doping into  $\alpha$ -B was only partial both for Li and Mg. The glittering look and the chemical shift of the EELS spectrum of the doped part suggest the metal transition by the doping. In only one sample, About 0.02 vol% of the doped part was found to be a superconductive phase with  $T_C$  of 36 K by the measurement of the temperature dependence of the magnetic susceptibility. On the other hand, we succeeded to dope Mg into  $\beta$ -B homogeneously by the VDP method up to 4 at% ( $\text{Mg}_{4.1}\text{B}_{105}$ ), though a considerable amount of Si was co-doped into the sample. On the first stage of the doping, mostly Mg was doped in but after 40 hrs doping, the Si ejected out the doped Mg. The Mg is doped at the D, E and F interstitial sites and the Si is doped at the  $A_1$  interstitial and B1 substitutional site. The expansions of the lattice are substantially due to the Mg-doping for the c-axis direction and the Si-doping for the a-axis direction. The concentration of the dopant and the lattice expansion have a linear correlation for the both Si- and Mg-doping. A temperature dependent component of the magnetic susceptibility, which obeys the Curie-Weiss law, was observed and the intensity of the component was proportional to the content of the doped Mg at D site, though the origin of the magnetism is not clear. Though superconductivity was not observed for the Mg-doped  $\beta$ -B, the results of the measurement of the EELS and the magnetic susceptibility suggests a metal transition of the  $\beta$ -B by the doping of more than 8 electrons/ $\text{B}_{105}$ , which are donated from the doped Si and Mg. This fact implies that the doped electrons filled up the intrinsic acceptor level with capacity of 8 electrons and the Fermi energy reached to the conduction band in the rigid band scheme of the  $\beta$ -B.

## Acknowledgement

The authors thank Prof. I. Higashi (Chiba Institute of Technology) for precious advises on the structural analysis, and Prof. H. Suematsu (University of Tokyo) and Mr. S. Sato (Cryogenic Center, University of Tokyo) for support of magnetic measurements using SQUID. This research was supported by the Mitsubishi Foundation and a Grants-in-Aid for Scientific Research from Japan Society for the Promotion of Science (JSPS).

## REFERENCES

- [1] M. Vlasse and J. C. Viala, *J. Solid State Chem.*, **37**, 181 (1981).
- [2] T. Lundström and L-E. Tergenius, *J. Less-Common Metals*, **82**, 341(1981).
- [3] S. Andersson and B. Callmer, *J. Solid State Chem.*, **10**, 219 (1974).
- [4] B. Callmer and T. Lundström, *J. Solid State Chem.*, **17**, 165 (1976).
- [5] T. Lundström, L-E. Tergenius and I. Higashi, *Z. Kristallogr.*, **167**, 235 (1984).
- [6] S. Andersson and T. Lundström, *J. Solid State Chem.*, **2**, 603 (1970).
- [7] I. Higashi, T. Sakurai and T. Atoda, *J. Less-Common Metals*, **45**, 283 (1976).
- [8] M. F. Garbaskas, J. S. Kasper and G. A. Slack, *J. Solid State Chem.*, **63**, 424 (1986).
- [9] I. Higashi and H. Iwasaki, *J. Solid State Chem.*, **82**, 230 (1989).
- [10] M. Kobayashi, I. Higashi, H. Matsuda and K. Kimura, *J. Alloys Compounds*, **221**, 120 (1995).
- [11] B. Callmer, L-E. Tergenius and J. O. Thomas, *J. Solid State Chem.*, **26**, 275 (1978).
- [12] B. Callmer, *J. Solid State Chem.*, **23**, 391 (1978).
- [13] H. K. Clark, *J. Amer. Chem. Soc.*, **65**, 2115 (1943).
- [14] E. Amberger and P. A. Rauh, *Acta Cryst. B*, **30**, 2549 (1974).
- [15] I. Higashi, M. Kobayashi, J. Bernhard, C. Brodhag and F. Thevenot, *AIP Conf. Proc.*, **231**, 201 (1991).
- [16] H. Matsuda, T. Nakayama, K. Kimura, Y. Murakami, H. Suematsu, I. Higashi and M. Kobayashi, *Phys. Rev. B*, **52**, 6102 (1995).
- [17] H. Matsuda, N. Tanaka, T. Nakayama, K. Kimura, Y. Murakami, H. Suematsu, and M. Kobayashi and I. Higashi, *J. Phys. Chem. Solids*, **57**, 1167 (1996).
- [18] T. Nakayama, H. Matsuda, K. Kimura and H. Ino, *J. Solid State Chem.*, **133**, 342 (1997).
- [19] T. Nakayama, J. Shimizu and K. Kimura, *J. Solid State Chem.*, **154**, 13 (2000).
- [20] H. Yamaguchi, Y. Sakairi, M. Takeda, K. Kimura and E. Matsubara, *Trans. Mater. Res. Soc. Jpn.*, **24**, 85 (1999).
- [21] M. Takeda, M. Ichimura, H. Yamaguchi, Y. Sakairi and K. Kimura, *J. Solid State Chem.*, **154**, 141 (2000).
- [22] S. Gunji and H. Kamimura and T. Nakayama, *J. Phys. Soc. Jpn.*, **62**, 2408 (1993).

- [23] S. Gunji and H. Kamimura, Phys. Rev. B, **54**, 13665 (1996)
- [24] M. C. Böhm, J. Schulte and R. Schlögl, Phys. Stat. Sol., **196**, 131(1996).
- [25] A. Oshiyama, S. Saito, N. Hamada and Y. Miyamoto, J. Phys. Chem. Solids, **53**, 1457 (1992)..
- [26] M. Z. Huang, Y. N. Xu and W. Y. Ching, Phys. Rev. B, **46**, 6572 (1992).
- [27] J. Nagamatsu, N. Nakagawa, T. Muranaka, Y. Zenitani and J. Akimitsu, Nature, **410**, 63 (2001).
- [28] J. M. An and W. E. Pickett, Phys. Rev. Lett., **86**, 4366 (2001).
- [29] H. J. Chol, D Roundy, H. Sun, M. L. Cohen and S. G. Loule, Nature, **418**, 758 (2002).
- [30] C. Wood and D. Emin, Phys. Rev. B, **29**, 4582 (1984).
- [31] J. A. Ugai and N. E. Soloviev, in Boron and Refractory Borides, ed. by V. I. Matkovich, Chap. CIII (Springer-Verlag, New York, 1977) pp. 227-240.
- [32] M. Terauchi, Y. Kawamata, M. Tanaka, M. Takeda and K. Kimura, J. Solid State Chem., **133**, 156 (1997).
- [33] F. Izumi and T. Ikeda, Mater. Sci. Forum, **321-324**, 198 (2000).
- [34] M. Terauchi, A. Oguri, and K. Kimura, to be submitted.
- [35] Y. Sato, M. Terauchi, A. Oguri, K. Soga and K. Kimura, to be submitted.
- [36] A. Oguri, K. Kimura, A. Fujiwara, M. Terauchi and M. Tanaka, AIP Conf. Proc., **590**, 507-510 (2001).
- [37] S. Brutti, M. Colapietro, G. Balducci, L. Barba, P. Manfrinetti and A. Palenzona, Intermetallics, **10**, 811 (2002).
- [38] G. A. Slack, C. I. Hejna, M. F. Garbaskas and J. S. Kasper, J. Solid State Chem., **76**, 52 (1988).
- [39] R. A. Young, "The Rietveld Method," ed. by R. A. Young (Oxford Univ. Press, Oxford, 1993), Chap. 1.
- [40] G. P. Tsiskarisvili, T. Lundstrom, L. Lundgren, G. V. Tsagareishvili, D. N. Tsikardze and F. N. Tavadze, J. Less-Common Metals, **147**, 41 (1989).
- [41] G. P. Tsiskarisvili, T. Lundstrom, L. Lundgren, G. V. Tsagareishvili, O. A. Tsagareishvili and F. N. Tavadze, J. Less-Common Metals, **142**, 91 (1988).



Table 1 Comparison between layered and cluster solids based on carbon and boron.

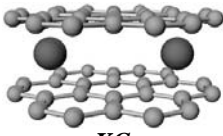
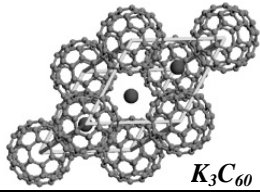
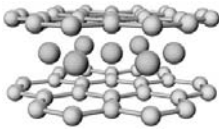
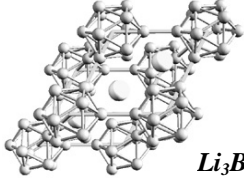
Major Component	Layered Solids	Cluster Solids
Carbon	<p><b>KC<sub>8</sub></b></p> <p><math>T_c \sim 0.1</math> K,  <math>N(E_F) \sim 14</math> states/eVnm<sup>3</sup></p>  <p><b>KC<sub>8</sub></b></p>	<p><b>K<sub>3</sub>C<sub>60</sub></b></p> <p><math>T_c \sim 20</math> K,  <math>N(E_F) \sim 25</math> states/eVnm<sup>3</sup></p> <p><b>Rb<sub>3</sub>C<sub>60</sub></b></p> <p><math>T_c \sim 30</math> K</p>  <p><b>K<sub>3</sub>C<sub>60</sub></b></p>
Boron	<p><b>MgB<sub>2</sub></b></p> <p><math>T_c \sim 40</math> K,  <math>N(E_F) \sim 24</math> states/eVnm<sup>3</sup></p>  <p><b>MgB<sub>2</sub></b></p>	<p><b>Li<sub>x</sub>B<sub>12</sub></b></p> <p><math>N(E_F) \sim 39</math> states/eVnm<sup>3</sup></p> <p><b>Mg<sub>x</sub>B<sub>12</sub></b></p> <p><b>Mg<sub>x</sub>B<sub>105</sub></b></p> <p><b>T<sub>c</sub> ?</b></p>  <p><b>Li<sub>3</sub>B<sub>12</sub></b></p>

Table 2 VDP conditions, lattice constants,  $a_{\text{hex}}$  and  $c_{\text{hex}}$  and volume,  $V$ , of the hexagonal unit cell in pure and (Mg, Si) doped  $\beta$ -rhombohedral boron. The values are listed in order of the length of lattice constant  $a_{\text{hex}}$ .

Sample name	VDP condition	$a_{\text{hex}}$ (Å)	$c_{\text{hex}}$ (Å)	$V$ (Å <sup>3</sup> )
$\beta$ -B	-	10.9270 $\pm$ 0.0008	23.828 $\pm$ 0.008	2463.9 $\pm$ 0.3
Mg- $\beta$ -1	1200 (°C) 10 (h)	10.980 $\pm$ 0.002	24.035 $\pm$ 0.004	2509.6 $\pm$ 0.7
Mg- $\beta$ -2	1200 (°C) 10 (h) 2 (times)	10.9880 $\pm$ 0.0008	24.084 $\pm$ 0.002	2518.2 $\pm$ 0.3
Mg- $\beta$ -3	1200 (°C) 10 (h) 3 (times)	10.998 $\pm$ 0.002	24.122 $\pm$ 0.004	2526.8 $\pm$ 0.9
Mg- $\beta$ -4	1200 (°C) 10 (h) 4 (times)	11.008 $\pm$ 0.002	24.130 $\pm$ 0.003	2532.2 $\pm$ 0.5
Mg- $\beta$ -5	1200 (°C) 10 (h) 5 (times)	11.0101 $\pm$ 0.0008	24.120 $\pm$ 0.002	2532.2 $\pm$ 0.3
Mg- $\beta$ -6	1200 (°C) 10 (h) 4 (times)	11.011 $\pm$ 0.001	24.122 $\pm$ 0.003	2532.9 $\pm$ 0.5
Mg- $\beta$ -7	1200 (°C) 10 (h) 6 (times)	11.021 $\pm$ 0.002	24.122 $\pm$ 0.003	2536.3 $\pm$ 0.6
Mg- $\beta$ -8	1200 (°C) 10 (h) 7 (times)	11.039 $\pm$ 0.001	24.111 $\pm$ 0.002	2544.5 $\pm$ 0.4
Mg- $\beta$ -9	1200 (°C) 40 (h)	10.958 $\pm$ 0.002	23.962 $\pm$ 0.003	2491.9 $\pm$ 0.8
Mg- $\beta$ -10	1200 (°C) 100 (h)	11.060 $\pm$ 0.001	23.990 $\pm$ 0.002	2541.2 $\pm$ 0.4
Mg- $\beta$ -11	1200 (°C) 200 (h)	11.0647 $\pm$ 0.0008	23.992 $\pm$ 0.002	2543.8 $\pm$ 0.3

Table 3 Occupancy of partial occupied positions in solid solutions of metals in  $\beta$ -rhombohedral boron.

Dopant	Atomic radius (Å)	Composition	Site occupancy (%)						Cell parameters			Ref.	
			A <sub>1</sub>	A <sub>2</sub>	D	D'	E	F	V (Å <sup>3</sup> )	a <sub>hex</sub> (Å)	c <sub>hex</sub> (Å)		
-	-	B <sub>105</sub>	-	-	-	-	-	-	-	2461.2	10.925	23.810	27
										~2465.3	~10.932	~23.819	
Si	1.17	SiB <sub>36</sub>	46.4	4.84	-	-	-	-	-	2509	11.01	23.90	1
Ge	1.225	GeB <sub>90</sub>	20.9	0.46	1.87	1.03	-	-	-	2481.8	10.958	23.862	2
Mn	1.24	MnB <sub>23</sub>	25.6	-	43.1	-	66.2	-	-	2508.8	10.988	23.994	3
Fe	1.241	FeB <sub>49</sub>	50.7	-	18.5	-	-	-	-	2478.1	10.951	23.861	4
Ni	1.246	NiB <sub>49</sub>	44.67	-	1.78	8.99	-	-	-	2482.21	10.9615	23.8544	5
Cr	1.249	CrB <sub>41</sub>	71.9	-	18.0	-	-	-	-	2482.5	10.9637	23.8477	6
Cu	1.278	CuB <sub>23</sub>	7.9	-	21	12	59.9	-	-	2500.2	10.985	23.925	7
Cu	1.278	CuB <sub>28</sub>	6.1	-	22.1	10.5	50.5	-	-	2489.9	10.9703	23.8898	3
V	1.321	VB <sub>65</sub>	64.0	-	5.3	-	-	-	-	2492.6	10.972	23.908	8
Al	1.431	AlB <sub>31</sub>	85.7	-	10.5	3.9, 3.9	-	-	-	2485.2	10.965	23.868	9
Li	1.52	LiB <sub>13</sub>	-	-	100	-	100	-	-	2504.3	10.9654	24.0495	10
Mg	1.60	MgB <sub>20</sub>	-	-	49.0	-	88.0	8.0	-	2523.5	10.983	24.156	30
Mg	1.60	MgSi <sub>0.05</sub> B <sub>26</sub>	11.9 (Si)	-	44.2 (Mg)	-	67.8 (Mg)	4.8 (Mg)	-	2526.8	10.998	24.122	*
Zr	1.60	ZrB <sub>51</sub>	-	-	27.9	-	18.1	-	-	2497.1	10.9564	24.0201	11
Sc	1.606	ScB <sub>28</sub>	-	-	31.4	-	72.7	-	-	2508.6	10.966	24.088	12

\* present study

Table 4 Reliability factor,  $R_{wp}$ , and occupancy of partially occupied site as results of Rietveld analysis on (Mg, Si) doped  $\beta$ -rhombohedral boron.

Sample name	Composition	Occupancy (%)							$R_{wp}$ (%)
		Si (A <sub>1</sub> )	Mg (D)	Mg (E)	Mg (F)	B (B <sub>4</sub> )	Si (B <sub>1</sub> )	B (B <sub>13</sub> )	
$\beta$ -B	B <sub>105</sub>	0	0	0	0	100	0	75	-
Mg- $\beta$ -1	Mg <sub>2.8</sub> Si <sub>0.13</sub> B <sub>105</sub>	5.0±0.5	32.7±0.4	48.6±0.5	0	100	0.6±0.3	75±1	10.4
Mg- $\beta$ -2	Mg <sub>4.1</sub> Si <sub>0.23</sub> B <sub>105</sub>	11.9±0.5	44.2±0.4	67.8±0.6	4.8±0.7	92±1	0.0	67±1	9.78
Mg- $\beta$ -3	Mg <sub>4.0</sub> Si <sub>0.44</sub> B <sub>105</sub>	2.7±0.5	43.3±0.4	64.6±0.6	4.4±0.5	80±1	6.8±0.4	57±1	9.33
Mg- $\beta$ -4	Mg <sub>4.1</sub> Si <sub>0.58</sub> B <sub>105</sub>	7.8±0.5	44.6±0.4	62.2±6	6.8±0.6	82±1	7.5±0.3	58±1	9.79
Mg- $\beta$ -5	Mg <sub>3.8</sub> Si <sub>0.70</sub> B <sub>105</sub>	8.3±0.4	42.4±0.4	54.2±0.6	6.4±0.6	80±1	9.4±0.3	57±1	9.12
Mg- $\beta$ -6	Mg <sub>3.8</sub> Si <sub>0.65</sub> B <sub>105</sub>	5.9±0.5	41.5±0.4	52.9±0.5	7.6±0.6	78±1	9.4±0.3	54±1	9.02
Mg- $\beta$ -7	Mg <sub>3.7</sub> Si <sub>0.80</sub> B <sub>105</sub>	7.6±0.5	42.0±0.4	49.9±0.6	5.3±0.6	83±1	11.4±0.3	58±1	9.36
Mg- $\beta$ -8	Mg <sub>3.2</sub> Si <sub>0.93</sub> B <sub>105</sub>	3.8±0.5	40.3±0.4	38.0±0.6	2.8±0.5	84±1	15.0±0.4	58±1	8.99
Mg- $\beta$ -9	Mg <sub>2.1</sub> Si <sub>0.43</sub> B <sub>105</sub>	22.8±0.4	17.5±0.3	43.6±0.5	5.0±0.7	83±1	0.0	68±1	10.1
Mg- $\beta$ -10	Mg <sub>1.5</sub> Si <sub>1.65</sub> B <sub>105</sub>	23.9±0.4	22.2±0.3	4.9±0.7	2.8±0.8	86±1	21.0±0.3	65±1	8.54
Mg- $\beta$ -11	Mg <sub>1.4</sub> Si <sub>1.78</sub> B <sub>105</sub>	23.3±0.5	21.4±0.3	0.0	2.9±0.9	92±1	23.3±0.4	68±1	9.07

Table 5 Temperature independent magnetic susceptibility,  $\chi_0$ , Currie constant,  $C$ , and Currie temperature,  $\theta_p$ , for the selected samples obtained by a fitting of eq. (3) to the experimental results.

Sample name	$\chi_0$ ( $10^{-7}$ emu/gOe)	$C$ ( $10^{-5}$ emu/gOe K)	$\theta_p$ (K)
$\beta$ -B (2N)	-9.2	6.7	-8.3
Mg- $\beta$ -1	-9.6	6.2	-3.3
Mg- $\beta$ -2	-9.2	8.3	-3.1
Mg- $\beta$ -3	-8.4	10	-3.5
Mg- $\beta$ -6	-7.3	9.3	-3.4
Mg- $\beta$ -8	-6.4	9.1	-3.6
Mg- $\beta$ -10	-6.8	5.8	-3.1

## FIGURE CAPTIONS

Fig. 1. VDP conditions for Li- and Mg-doping into  $\alpha$ -B. The conditions indicated by arrows are those for the samples used for the EELS measurement.

Fig. 2. XRD patterns of un-doped, Li- and Mg-doped  $\alpha$ -B.

Fig. 3. EELS spectra of un-doped, Li- and Mg-doped  $\alpha$ -B (a) [34]. The arrows indicate the stepwise increase of the signal described in the text. (b) shows the results of first-principle calculation by Gunji et al. [23].

Fig. 4. Temperature dependence of magnetic susceptibility of un-doped and Li-doped  $\alpha$ -B (Li- $\alpha$ -1) under zero-field cool (ZFC) and field cool (FC).

Fig. 5. Dependence of magnetization of un-doped and Li-doped  $\alpha$ -B on the strength of the applied magnetic field. The values at 100 K is subtracted from those at 20 and 37.5 K to eliminated the effects of ferromagnetic impurities.

Fig. 6. XRD patterns of un-doped and Mg-doped  $\beta$ -B.

Fig. 7. Dependence of site occupancy on total doping time for Mg-doped  $\beta$ -B.

Fig. 8. Schematic illustration of the dope sites in  $\beta$ -B ( $B_{105}$ ).

Fig. 9. Relation between dopant contents and the cell expansion of  $\beta$ -B in a-axis (a) and c-axis (b) direction. (c) shows the correlation between observed lattice parameters and calculated ones by eq. (2).

Fig. 10. EELS spectra of un-doped  $\beta$ -B and samples Mg- $\beta$ -1, 3 and 8 [35]. The arrows indicate the stepwise increase of the signal described in the text.

Fig. 11. Temperature dependence of magnetic susceptibility of un-doped and Mg doped  $\beta$ -B (a). (b) is magnified plots to show the negative values at a room temperature.

Fig. 12. Relation between Currie constant and the square of dopant content. Dashed line crossing the origin shows the linearity of the Currie constant on the dopant content for Mg at D site.

Fig. 13. Relation between number of doped electrons and the  $\Delta N(E_F)$  calculated from the results of magnetic susceptibility measurement.

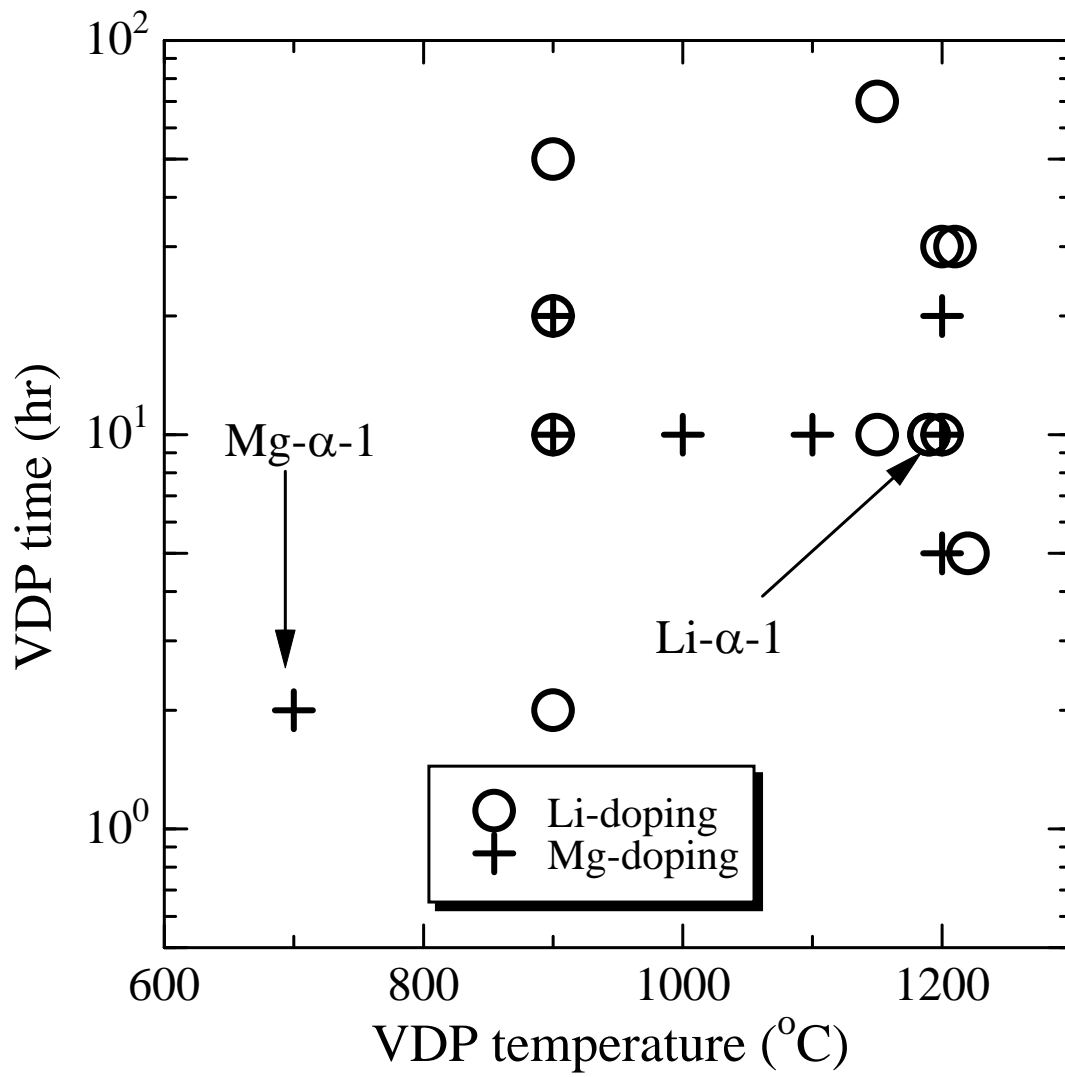


Fig. 1. VDP conditions for Li- and Mg-doping into  $\alpha$ -B. The conditions indicated by arrows are those for the samples used for the EELS measurement.

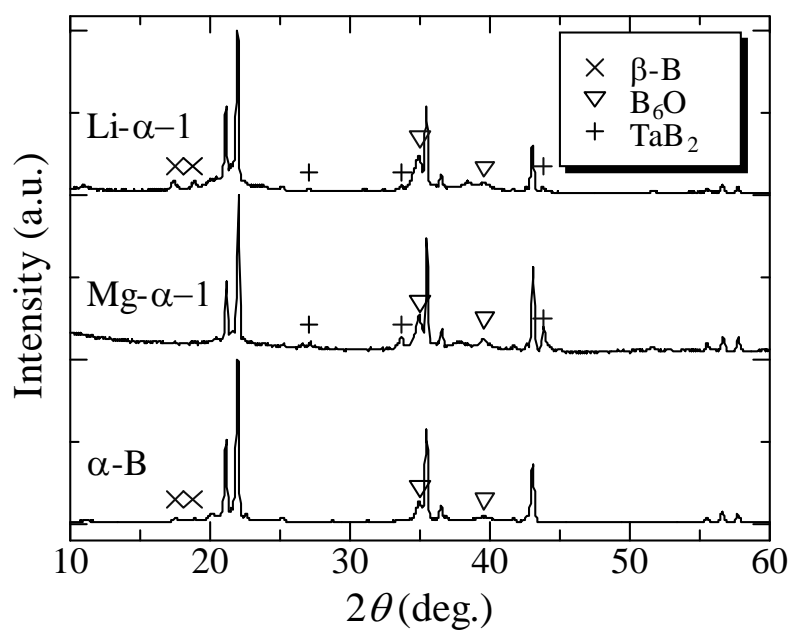


Fig. 2. XRD patterns of un-doped, Li- and Mg-doped  $\alpha$ -B.



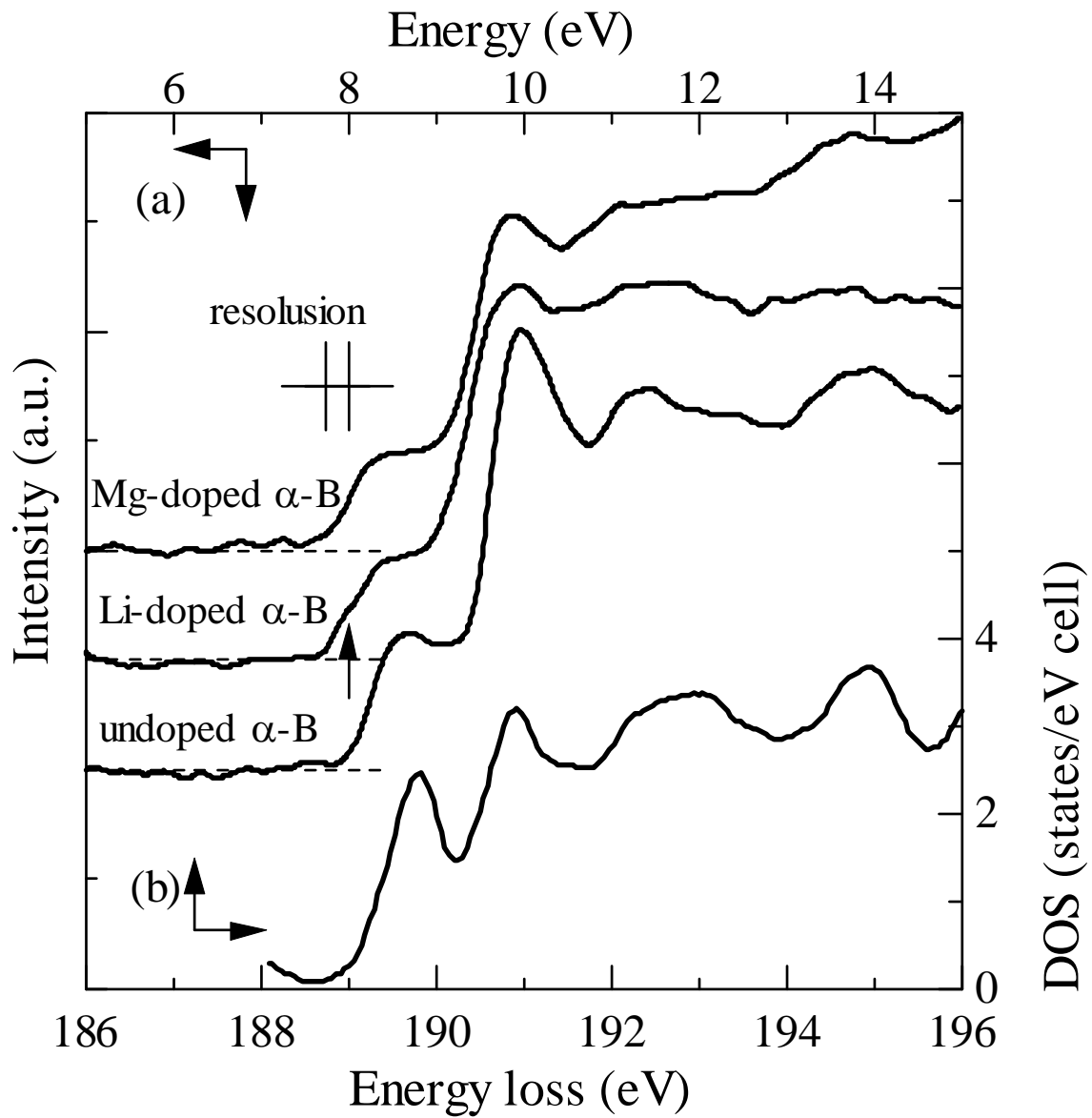


Fig. 3. EELS spectra of un-doped, Li- and Mg-doped  $\alpha$ -B (a) [34]. The arrows indicate the stepwise increase of the signal described in the text. (b) shows the results of first-principle calculation by Gunji et al. [23].

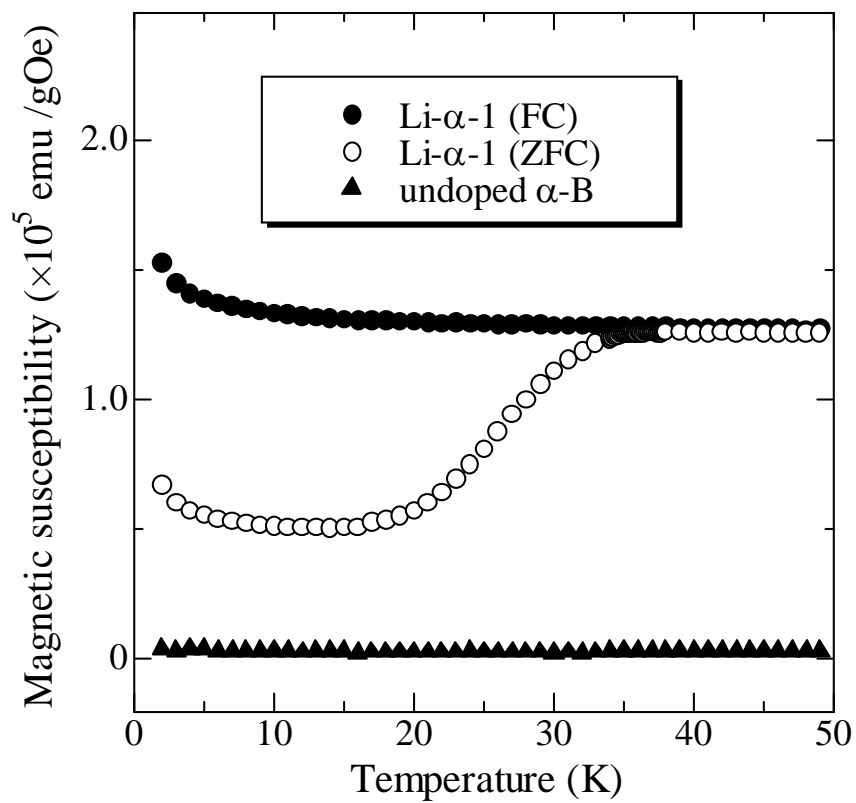


Fig. 4. Temperature dependence of magnetic susceptibility of un-doped and Li-doped  $\alpha$ -B (Li- $\alpha$ -1) under zero-field cool (ZFC) and field cool (FC).

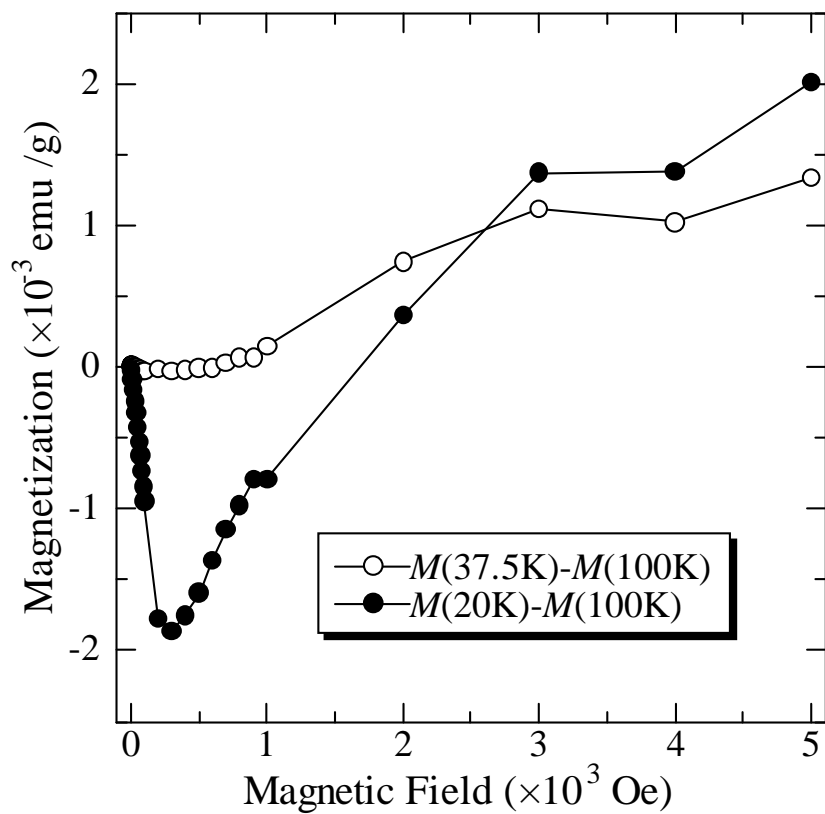


Fig. 5. Dependence of magnetization of un-doped and Li-doped  $\alpha$ -B on the strength of the applied magnetic field. The values at 100 K is subtracted from those at 20 and 37.5 K to eliminated the effects of ferromagnetic impurities.

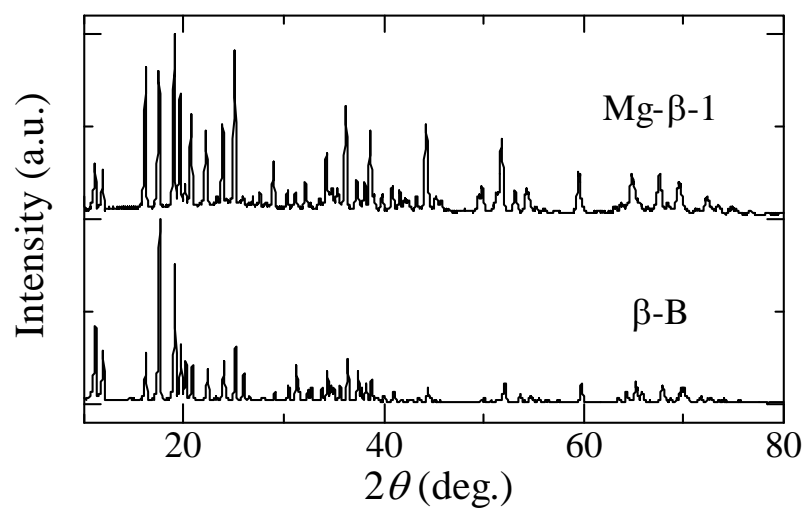


Fig. 6. XRD patterns of un-doped and Mg-doped  $\beta$ -B.

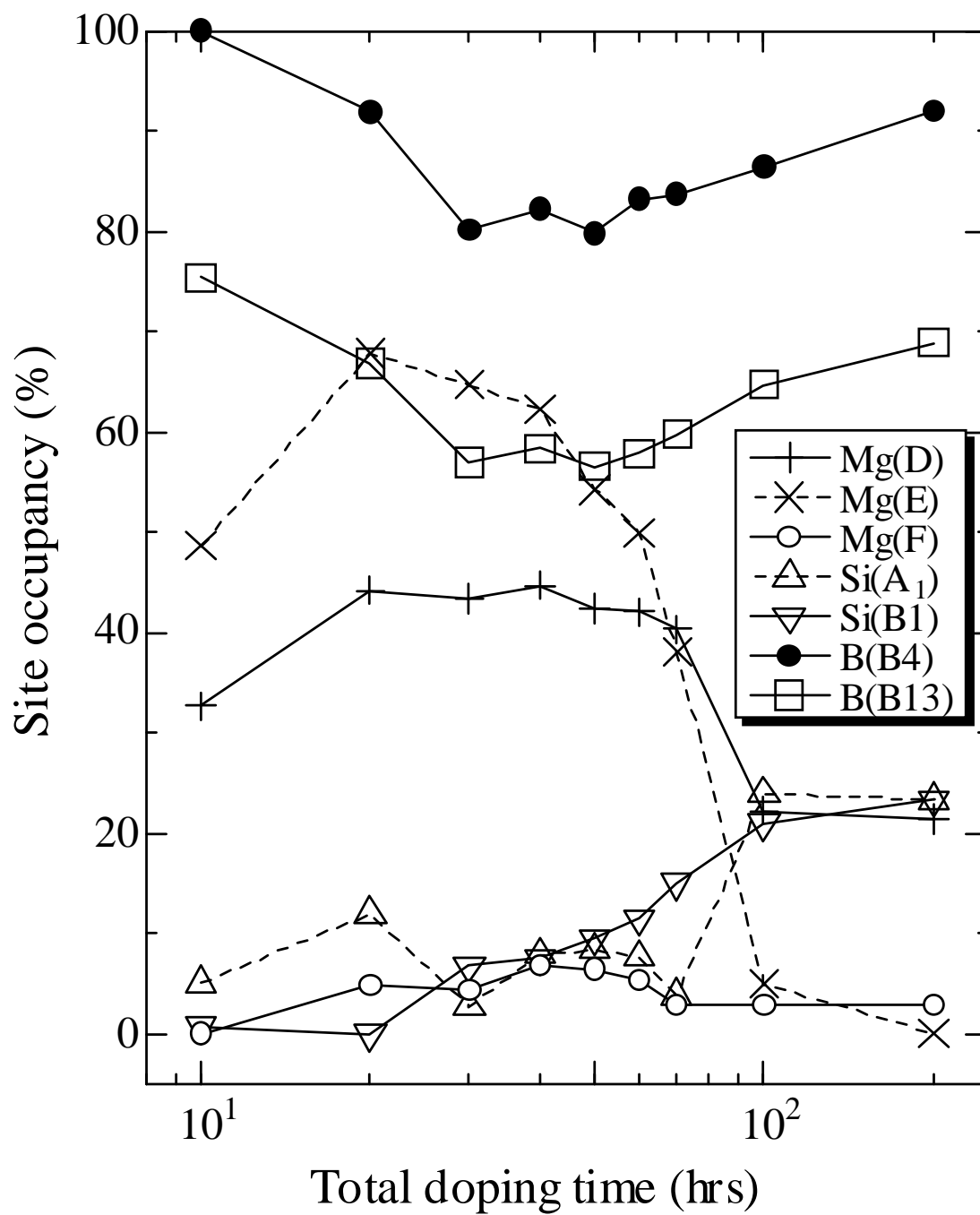
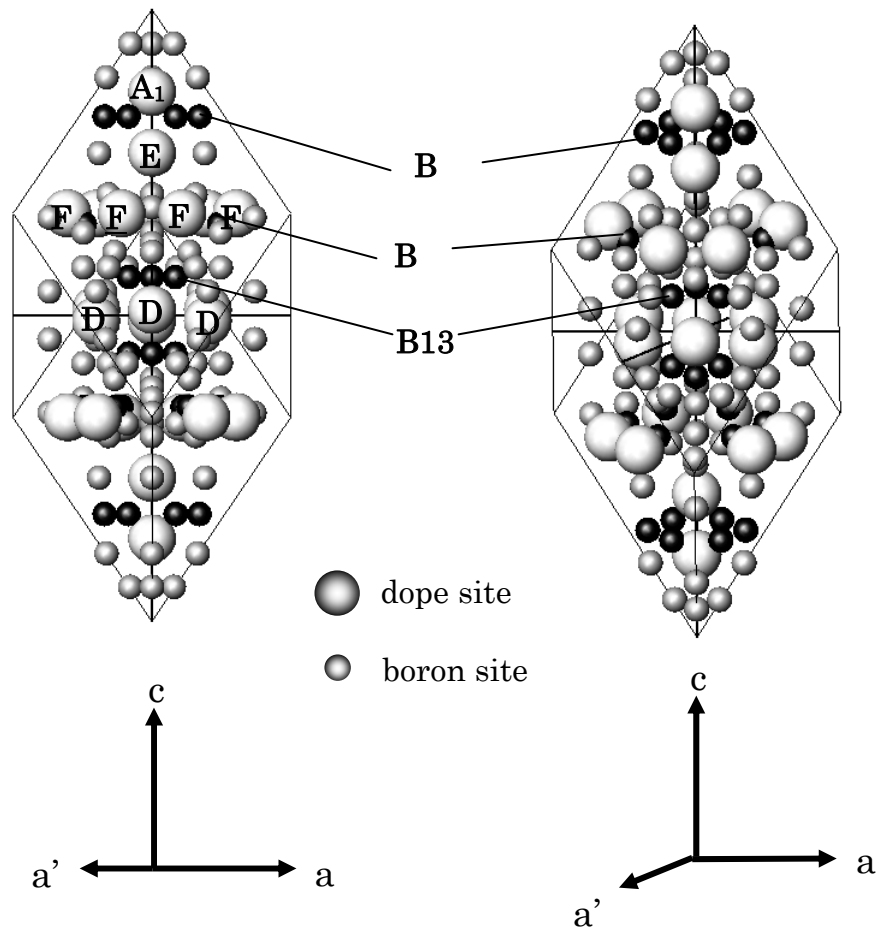


Fig. 7. Dependence of site occupancy on total doping time for Mg-doped  $\beta$ -B.



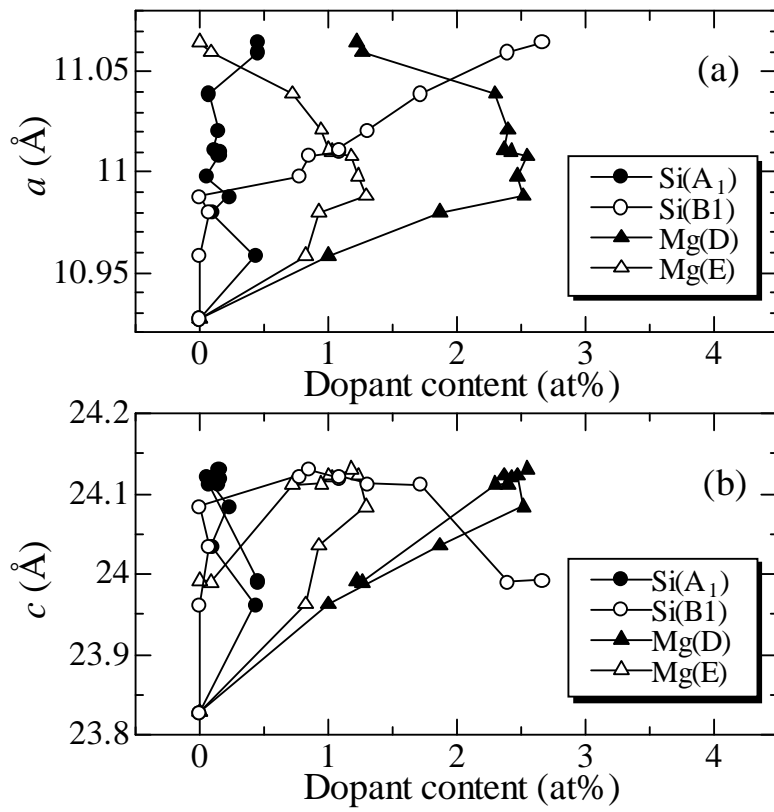


Fig. 9. Relation between dopant contents and the cell expansion of  $\beta$ -B in a-axis (a) and c-axis (b) direction. (c) shows the correlation between observed lattice parameters and calculated ones by eq. (2).

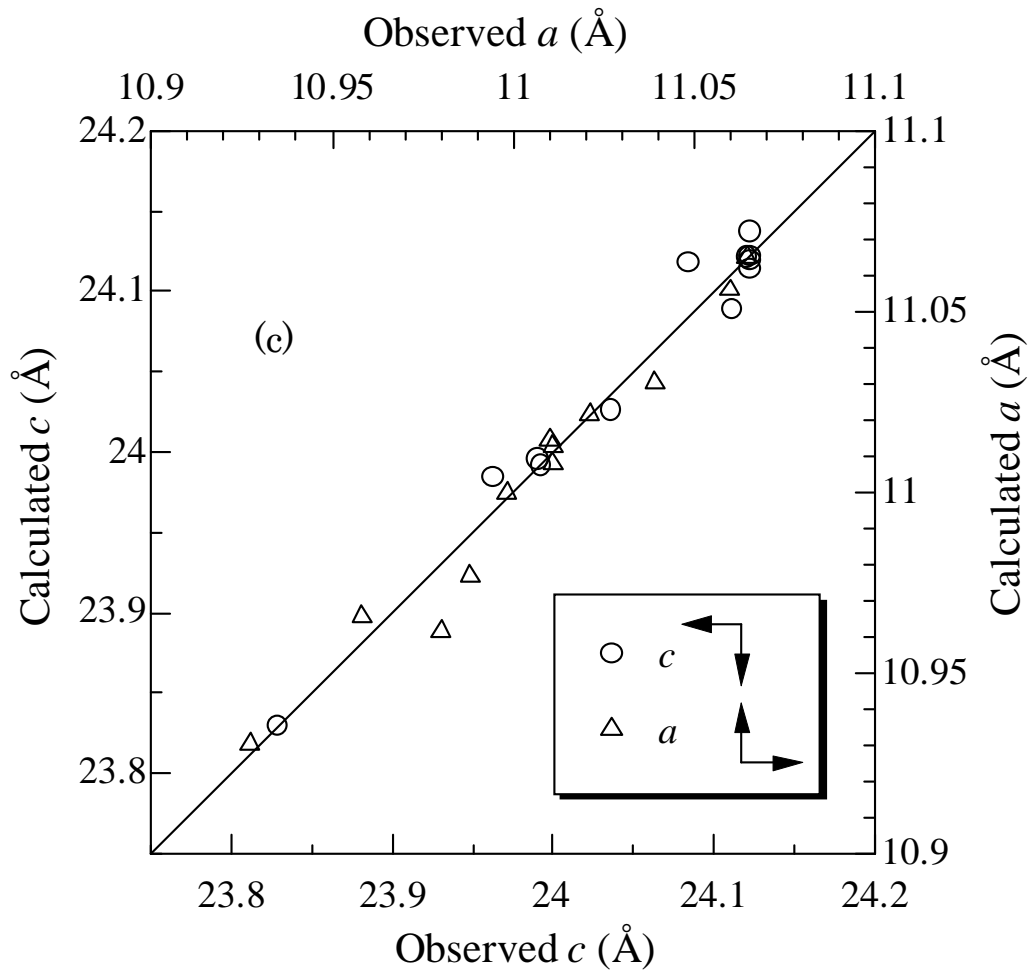


Fig. 9. Relation between dopant contents and the cell expansion of  $\beta$ -B in a-axis (a) and c-axis (b) direction. (c) shows the correlation between observed lattice parameters and calculated ones by eq. (2).



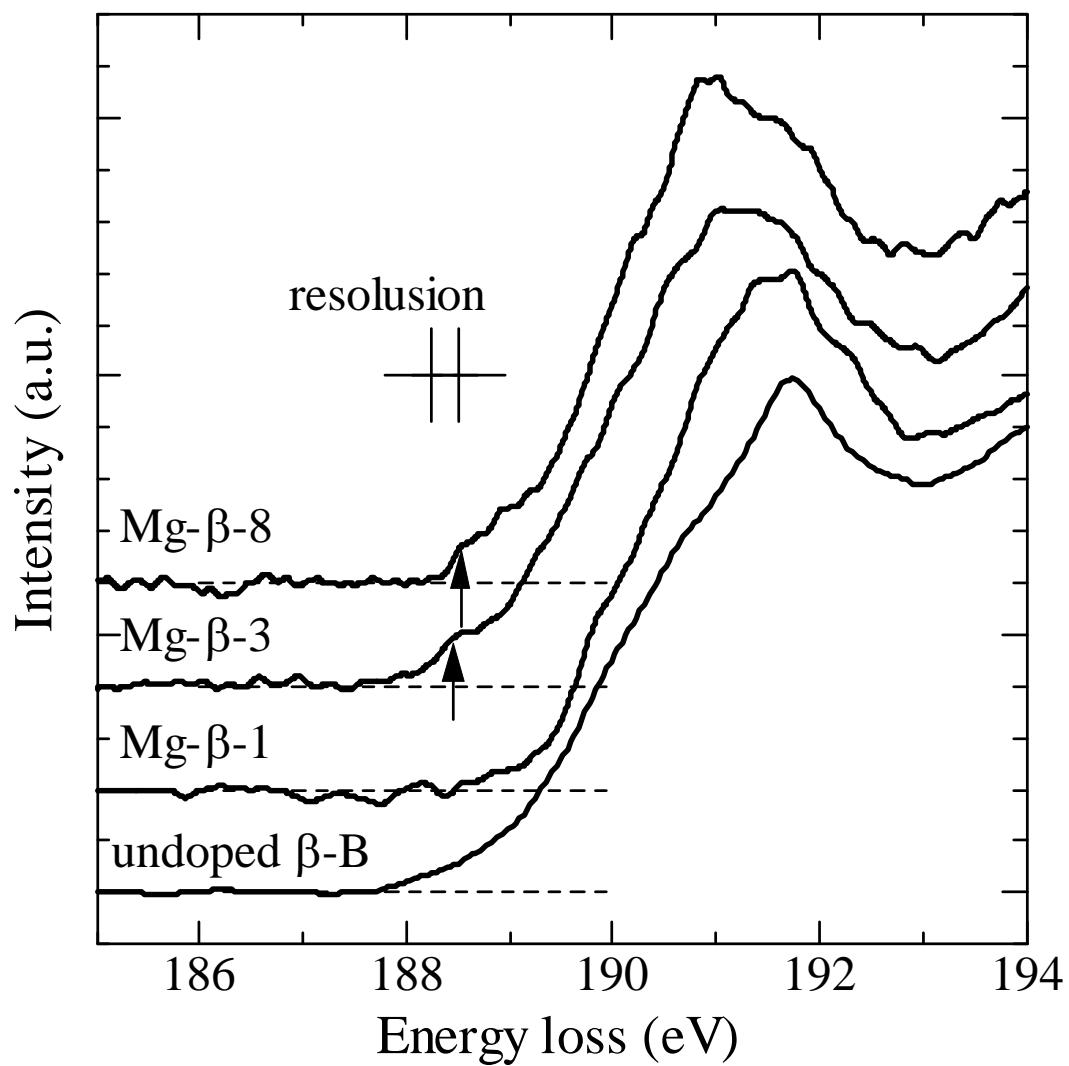


Fig. 10. EELS spectra of un-doped  $\beta$ -B and samples Mg- $\beta$ -1, 3 and 8. The arrows indicate the stepwise increase of the signal described in the text.

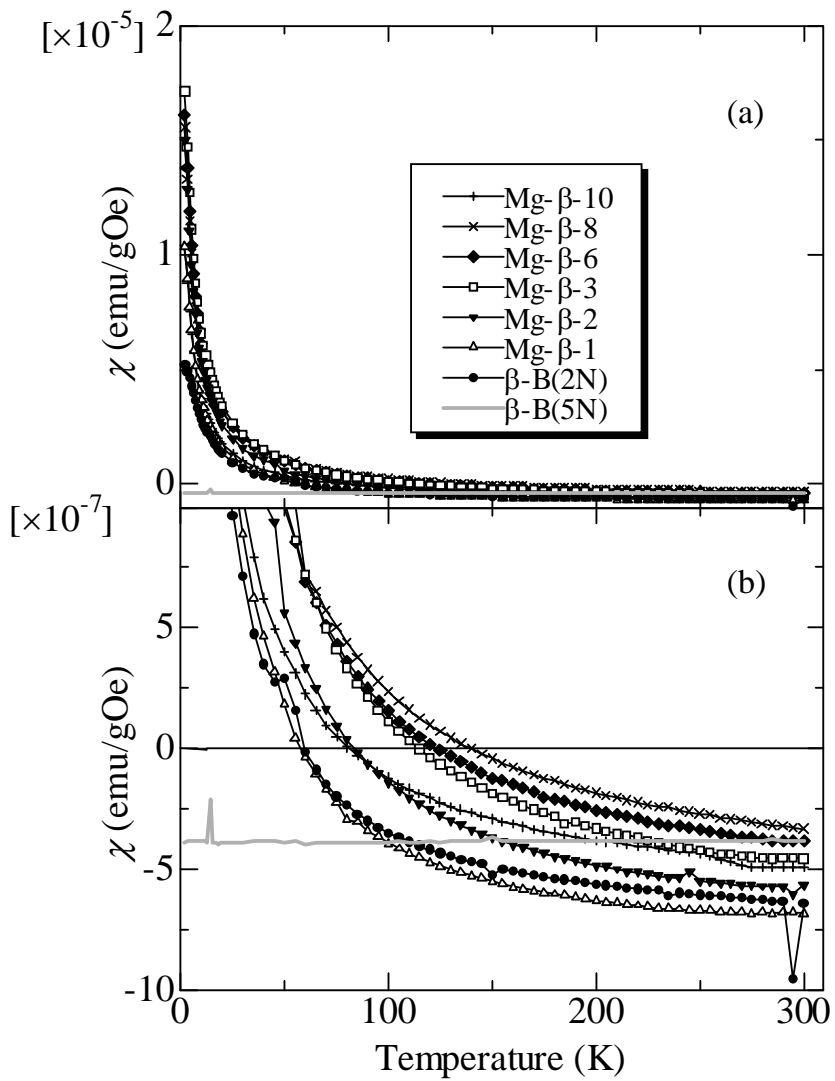


Fig. 11. Temperature dependence of magnetic susceptibility of un-doped and Mg doped  $\beta$ -B (a). (b) is magnified plots to show the negative values at a room temperature.

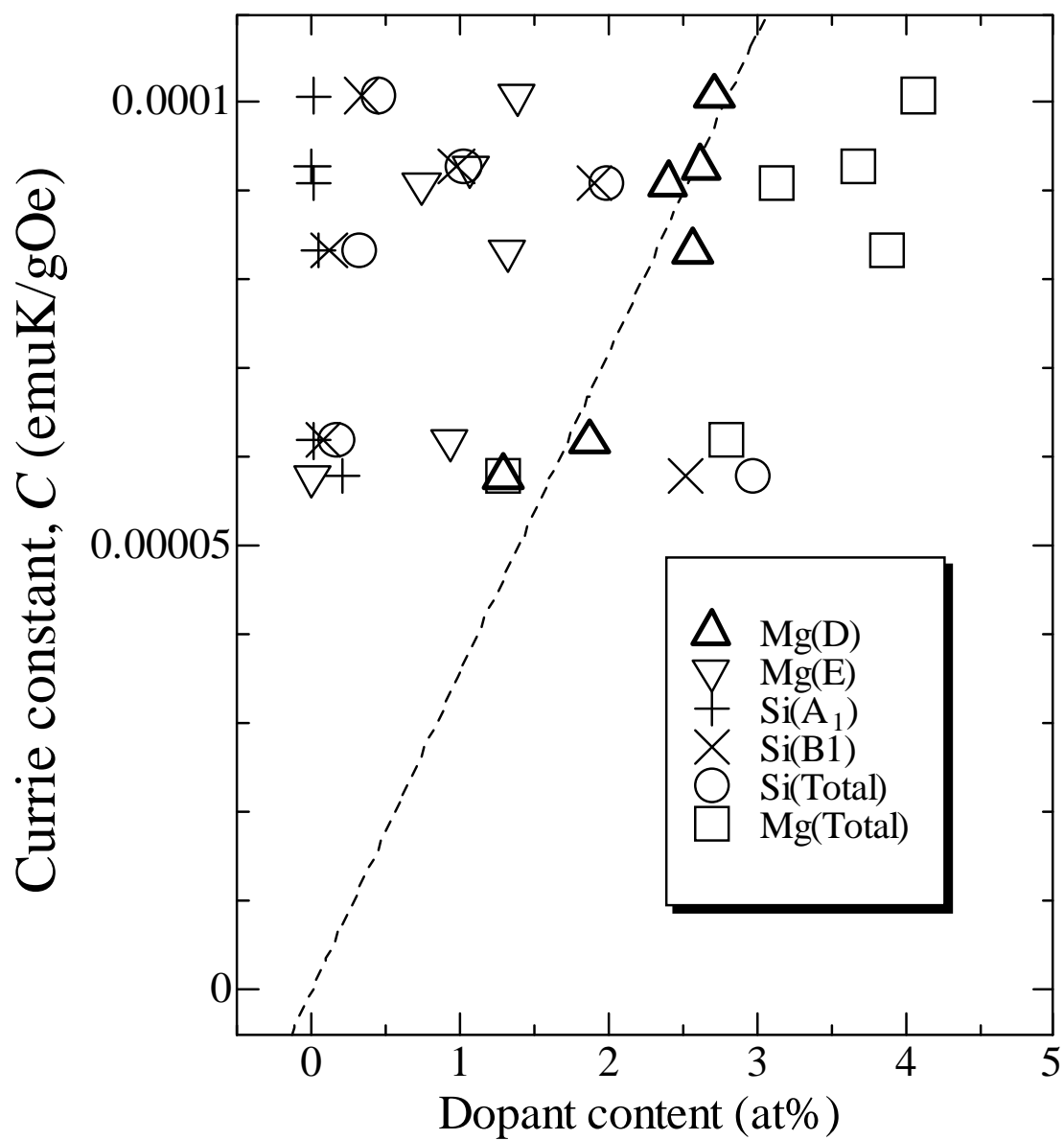


Fig. 12. Relation between Currie constant and the square of dopant content. Dashed line crossing the origin shows the linearity of the Currie constant on the dopant content for Mg at D site.

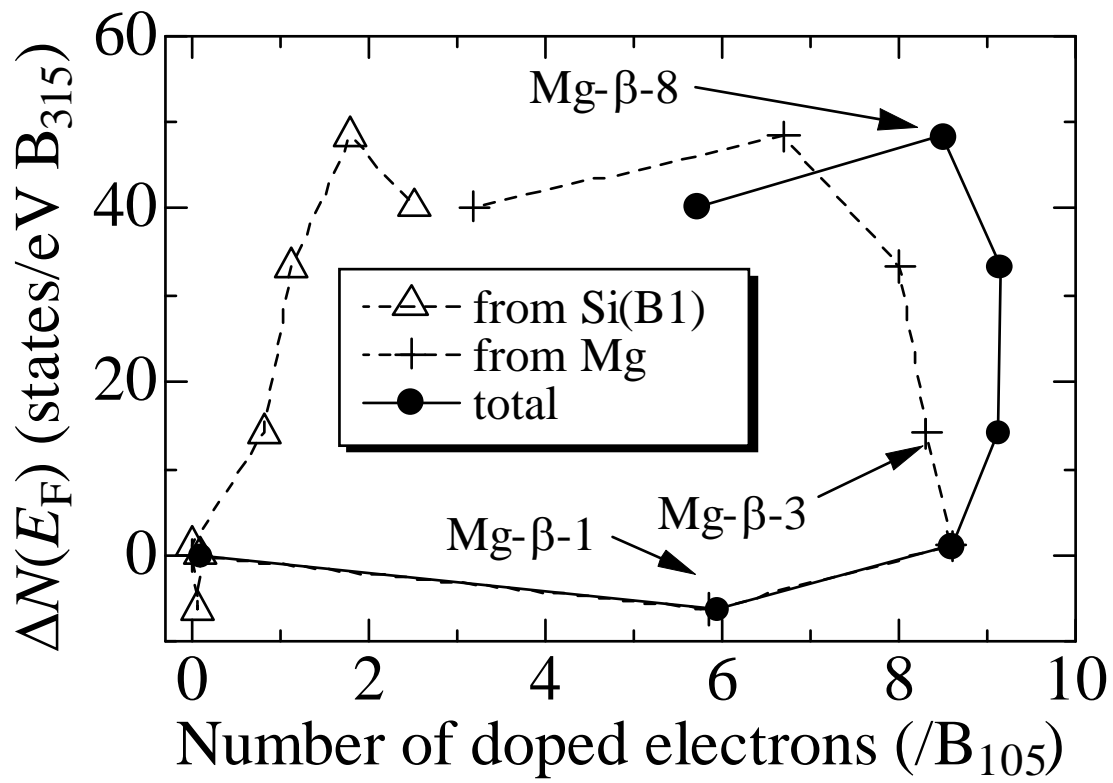


Fig. 13. Relation between number of doped electrons and the  $\Delta\mathcal{N}(E_F)$  calculated from the results of magnetic susceptibility measurement.